J Membrane Biol (2007) 219:19–36
DOI 10.1007/s00232-007-9058-4

Time-Dependent Molecular Memory in Single Voltage-Gated Sodium Channel

Tapan K. Nayak · S. K. Sikdar

Received: 12 February 2007 / Accepted: 18 June 2007 / Published online: 1 September 2007

Abstract Excitability in neurons is associated with firing of action potentials and requires the opening of voltage-gated sodium channels with membrane depolarization. Sustained membrane depolarization, as seen in pathophysiological conditions like epilepsy, can have profound implications on the biophysical properties of voltage-gated ion channels. Therefore, we sought to characterize the effect of sustained membrane depolarization on single voltage-gated Na^+ channels. Single-channel activity was recorded in the cell-attached patch-clamp mode from the $rNa_v1.2\alpha$ channels expressed in CHO cells. Classical statistical analysis revealed complex nonlinear changes in channel dwell times and unitary conductance of single Na^+ channels as a function of conditioning membrane depolarization. Signal processing tools like weighted wavelet Z (WWZ) and discrete Fourier transform analyses attributed a "pseudo-oscillatory" nature to the observed nonlinear variation in the kinetic parameters. Modeling studies using the hidden Markov model (HMM) illustrated significant changes in kinetic states and underlying state transition rate constants upon conditioning depolarization. Our results suggest that sustained membrane depolarization induces novel nonlinear properties in voltage-gated Na^+ channels. Prolonged membrane depolarization also induced a "molecular memory" phenomenon, characterized by clusters of dwell time events and strong autocorrelation in the dwell time series similar to that reported recently for single enzyme molecules. The persistence of such molecular memory was found to be dependent on the duration of depolarization. Voltage-gated Na^+ channel with the observed time-dependent nonlinear properties and the molecular memory phenomenon may determine the functional state of the channel and, in turn, the excitability of a neuron.

Keywords Voltage-gated sodium channel · Cell-attached patch-clamp · Conditioning depolarization · Pseudoperiodic oscillation · Autocorrelation · Molecular memory

T. K. Nayak · S. K. Sikdar (✉)
Molecular Biophysics Unit, Indian Institute of Science, Bangalore-12, India
e-mail: sks@mbu.iisc.ernet.in

Introduction

Spike timing, delay and information coding in the nervous system largely depend on the availability of voltage-gated Na^+ conductance and the "conformational preparedness" of the channel at the molecular level. The availability of Na^+ conductance is the outcome of a complex interplay between activation, inactivation and recovery from inactivation processes of Na^+ channel (Mickus, Jung & Spruston, 1999; Ong, Tomaselli & Balser, 2000; Goldin, 2003). The dynamics of voltage-gated Na^+ channel inactivation and recovery thereof are complex nonlinear functions of the amplitude and duration of depolarization (Toib, Lyakhov & Marom, 1998; Majumdar, Foster & Sikdar, 2004). Neuronal membranes can remain depolarized (above threshold) for varying and extended time durations in conditions such as epileptic seizures (Rutecki & Yang, 1998), brain ischemia (Xu, 1995), pain (Wu et al., 2005) and during spontaneous network activity observed in working memory within local circuits (McCormick et al., 2003). Epileptic seizures are known to bring about acquired changes in somatic ion channels (Chen et al., 2001; Su et al., 2002). This raises an intriguing question involving the possible role of sustained depolarization in inducing dynamic conformational changes in voltage-gated Na^+ channel molecules. Such changes in

Na^+ channel molecules can affect the input-output relationship of the neuron, leading to altered excitability (Reyes, 2001). Changes in intrinsic molecular properties of neurons have been reported to occur independently of synaptic components, which is the basis of intrinsic neuronal plasticity (Tsubokawa et al., 2000). Dynamic time-dependent changes in single-Na^+ channel kinetics can potentially determine intrinsic neuronal plasticity. Recent studies on enzyme kinetics illustrate a substrate concentration-dependent memory effect in single-enzyme molecules, which is attributed to internal conformational fluctuations (English et al., 2005; Lerch, Rigler & Mikhailov, 2005; Vlad et al., 2002). Tetrodotoxin-sensitive sodium channels $Na_v1.1$ and $Na_v1.2$ are ubiquitously distributed in the central nervous system and have been strongly implicated in neuronal signal processing, epilepsy (Segal, 1994; Kohling, 2002), brain ischemia (Katsumata et al., 2003) and neuropathic pain (Amir et al., 2002; Waxman et al., 1999). Therefore, in the current work we sought to characterize the effect of sustained membrane depolarization on the molecular behavior of a single voltage-gated Na^+ channel, $rNa_v1.2$, and explore the possible existence of a depolarization duration-dependent molecular memory phenomenon in analogy to single-enzyme molecules.

We performed cell-attached single-channel patch-clamp recordings of the rat brain type IIA voltage-gated sodium channel α-subunit (rNav1.2α) heterologously expressed in Chinese hamster ovary (CHO) cells. Here, we show a profound effect of sustained depolarization on channel dwell times by conventional statistical treatment of the open, shut and first latency time distributions, which show nonlinear dependence on the duration of conditioning depolarization. Quantitative analyses of the nonlinear changes in the channel kinetic parameters using weighted wavelet Z (WWZ) transform and discrete Fourier transform (DFT) analyses attributed a "pseudo-oscillatory" nature to the nonlinearity. The sodium channel unitary conductance showed significant changes and a strong inverse correlation with first latency following sustained depolarization. Kinetic modeling using hidden Markov modeling (HMM) of the raw single-Na^+ channel current traces suggested that the underlying state sequences as well as the kinetic rate constants for state transitions undergo nonlinear changes with varying durations of conditioning depolarization. Autocorrelation analysis of series of dwell times revealed the induction of significant correlation in channel activity temporally following varying conditioning pulses. Following longer durations of depolarization, the dwell times seemed to become more clustered, i.e., longer dwell times following longer ones and smaller dwell times following smaller ones. This was suggestive of a time-dependent molecular memory phenomenon in the Na^+ channel molecule. The persistence of such a memory phenomenon was found to be dependent on the duration of conditioning depolarization. Our results suggest that sustained depolarization can have a profound effect on the properties of voltage-gated Na^+ channels manifested as the observed nonlinear properties and the induction of a novel memory phenomenon in the molecule.

Materials and Methods

Electrophysiological Measurements

A single sodium channel current was recorded from rNav1.2α stably expressed in CHO cells (CNa18 cell line [Sarkar, Adhikari & Sikdar, 1995]) as described earlier (Majumdar et al., 2004). Cell-attached gigaohm seals were obtained using fire-polished borosilicate micropipettes (Clark Electromedical Instruments, Kent, UK) of 5–10 MΩ resistance, whose tips were coated with Sylgard (General Electric company, New York) to reduce capacitive noise (Sigworth & Neher, 1980; Hamill et al., 1981). For cell-attached recordings, the pipette solution contained (in mM) NaCl 135, $CaCl_2$ 1.5, $MgCl_2$ 1 and 4-(2-hydroxyethyl)-1-piperazineethanesulfonic acid (HEPES) 10 (pH 7.4 adjusted with NaOH), and the bath solution contained (in mM) K^+ gluconate 135, $CaCl_2$ 1.5, $MgCl_2$ 1 and HEPES 10 (pH 7.4) adjusted with KOH (Berman et al., 1989). The holding potential for all the experiments was –90 m*V*, and the temperature of the bath was maintained at 15°C.

Single-channel current recordings were acquired (sampling rate 50 kHz, analog seven-pole Bessel filter with filter cut-off 3 kHz) using an EPC8 amplifier (HEKA Instruments, Lambrecht, Germany), digitized using an LIH 1600 A/D converter (HEKA Electronik, Lambrecht, Germany) and analyzed using the Pulse (HEKA Electronik, Lambrecht, Germany), TAC (Bruxton Corp., Seattle, WA), WCP and PAT (John Dempster, University of Strathclyde, Glasgow, UK) programs. However, for automated event detection a digital gaussian filter of 1.5 KHz, incorporated in the single-channel analysis software, was additionally used.

A two-pulse protocol with a variable conditioning pulse of 0–1,200 ms (-10 m*V*) followed by a test pulse of 40 ms (−10 m*V*) with an intervening recovery period of 80 ms was used to study the effects of sustained depolarization on the single-channel dwell times (*see below*, Fig. 3a). To examine the effect of conditioning depolarization on single-channel conductance, currents were recorded at different test pulse potentials, ranging from −50 to 40 m*V*, before and after a variable conditioning pulse. After the application of each pulse protocol, sufficient time was allowed (3–5 min) for the channel to recover from the effect of the previous protocol; and while studying the effect of progressively increasing conditioning pulses, the

pulse protocols were randomized so that there would be no stimulus or time-related artifacts. The single-channel current amplitudes in cell-attached patches in our case generally remained stable for almost 60–90 min, which was often verified by constructing stability plots (*see* Fig. 8c).

Data Analysis

Digitized single-channel current records were corrected for leak and capacitive transients by subtracting the averaged current traces having no channel activity. Automated single-channel event detection was performed after setting a threshold at half the maximum open channel current amplitude (Colquhoun & Sigworth, 1983). Amplitude histograms were constructed and fitted to gaussian functions to determine the single-channel current amplitudes (Colquhoun & Sigworth, 1983). Dwell time distribution histograms were obtained by plotting the number of events against the appropriately binned time interval. Cumulative distribution histograms were constructed from the dwell time distribution histograms. A maximum likelihood method was used to fit the histograms with a sum of exponential cumulative distribution functions (cdfs) to yield the mean dwell times or the time constants (τ_{latency},τ_{open}) (Colquhoun & Sigworth, 1983; Sachs, Neil & Barkakati, 1982). The filter dead time was estimated to be 80 μs at a filter frequency of 1,500 Hz. To avoid error due to missed events, the first bin (bin width 0.08–0.16 ms) was ignored for fitting the exponential cdfs. The fitting of dwell time histograms by exponential functions was always qualified by the chi-squared test. While fitting, the model with fewer parameters was always statistically preferred (law of parsimony). Statistical analyses on the data were done using Sigma Plot 4.0 (Systat Software Inc., San Jose, CA), Graph Pad and Graph Pad Prism software (GraphPad, San Diego, CA). Analyses were done only on patches having one or two channels, indicated by the number of overlapping openings. For the analysis of patches containing more than one channel, appropriate correction was applied (Patlak & Horn, 1982; Aldrich, Corey & Stevens, 1983) as follows:

$$p_n(t) = 1 - (1 - f(t))^n \tag{1}$$

where p_n is the probability of a channel opening at time t when there are n independent channels in the patch and $f(t)$ is the first latency distribution function for a patch containing only one channel.

Fourier and Wavelet Analysis

The time series obtained from the distribution of time constants (τ_{latency}, τ_{open}) associated with channel kinetics were quantified for component frequencies by Fourier transform and wavelet analysis. The process of writing any function $x(t)$ in terms of periodic complex exponential functions, thus "deconvoluting" $x(t)$ into $x(f)$, where t and f are time and frequency, respectively, is known as the "Fourier transform" (FT). FT analysis of the data was done using the Time Series program (TS, Foster G, 1995, http://www.AAVSO.org), which computes the DFT of the data. It also computes the inverse FT using the statistically significant frequencies to generate a model curve to fit the data. As FT does not resolve the time domain of component frequencies in the time series, WWZ transform analysis (Foster G, 1996, http://www.AAVSO.org) was used to obtain the time stamps of the statistically significant frequencies (Majumdar et al., 2004; Majumdar & Sikdar, 2005). In wavelet transform, a given time series was scanned by a size variable basic or "mother wavelet," by moving it through the time series. In the process, all possible sizes of the mother wavelet were used to find out when the time series behaved as the wavelet, thereby resolving the time domain. At the same time, the frequency domain was resolved by varying the scale of the mother wavelet without changing the shape. This is explicitly expressed as follows:

$$\gamma(s,\tau) = \frac{1}{\sqrt{s}} \int f(t)\psi_{s,\tau}\left(\frac{t-\tau}{s}\right)dt \tag{2}$$

where, $\psi_{s,\tau}$ is the basic mother wavelet and s and τ are the scaling and translation variables, respectively, which help determine the frequency and the time of occurrence of a particular frequency in the time series. The information was displayed by three-dimensional (3D) or contour plot where the x axis represented the time, the y axis represented the frequency and the z axis represented the Z-statistics score assigned to the statistically significant frequencies in the time series. For DFT and wavelet analysis, frequencies higher than 10 Hz were ignored.

HMM Analysis

HMM was used to analyze the kinetics of single sodium channels using the raw single-channel current traces from patches containing only one channel. The single-channel data are considered "hidden" because the underlying state sequences are not directly observed at any given time since multiple states may share the same conductance and due to the background noise. HMM analysis was carried out using the method developed by Venkataramanan et al. (Venkataramanan, Kuk & Sigworth, 1998, 2000; Zheng, Venkataramanan & Sigworth, 2001), with the HMM analysis code integrated into the TAC program (Sunderman & Zagotta, 1999). It models the single-channel activity as two components: (1) a "noiseless" signal representing the

current levels of the conducting states as the channel makes transitions from one state to another and (2) background gaussian noise. The method distinguishes between actual events and background noise in a more sophisticated manner than is possible by the half-amplitude threshold crossing method. The algorithm uses an extension of the forward-backward algorithm and the Baum-Welch optimization algorithm. The HMM approach uses inverse filtering to substitute a sharp roll-off filter with corner frequency fixed at 0.4 × the sampling frequency for the gradual seven-pole Bessel filter that was used to record the data. Thus, in our case, with data recorded with the Bessel filter set at 3 kHz and sampling frequency of 50 KHz, the effect of inverse filtering was to effectively replace the 3-kHz filter and impose a sharp cut-off filter with a corner frequency of 20 kHz. Because of the inverse filtering, the effective bandwidth increases approximately sixfold, making it possible to detect short-duration events and obtain estimates of fast rate constants (Sunderman & Zagotta, 1999; Venkataramanan & Sigworth, 2002), which were previously missed. Due to inverse filtering, the sampling frequency, 50 kHz, becomes 1.25 times that of the Nyquist frequency, 40 kKHz, thereby enabling us to overcome the problem of oversampling. The inverse filtering is based on the step response of the acquisition system, which was acquired by configuring Pulse to output voltage steps, converting the voltage signal to current and then feeding the current signal directly to the head stage of the patch-clamp amplifier. Several such responses were recorded, averaged and processed to obtain the step response of the amplifier system (Venkataramanan & Sigworth, 2002). For HMM analysis, the complete trace of 40 ms duration was selected (*see* Fig. 7a), which represented the first latency, open and inactivation states of the channel. Approximately 2,000 data points per trace were selected, and in each recording about 150 traces were used for the analysis. In each of the models, four autoregressive coefficients were used, which were calculated approximately by simulating a one-state model on traces containing no channel activity. The HMM analysis took three inputs: (1) raw data after inverse filtering; (2) an HMM model containing information regarding the underlying states, state transitions, underlying noise in each state and autoregressive coefficients; and (3) an events list obtained by an automated event detection tool. The program was run with the "continuous time option," and the relative log likelihood (RLL) scores obtained from the simulation were used to rank the models and find the most appropriate model for different conditioning pulse durations. The accuracy of the HMM analysis was confirmed by using the idealized event list produced by the model to draw the dwell time distribution histograms in TAC FIT and comparing the results with those obtained by the half-amplitude threshold crossing method (*see* Fig. 7c).

Autocorrelation Analysis

To substantiate the induction of the molecular memory phenomenon due to conditioning depolarization, autocorrelation analysis was performed. A series of single-channel dwell times (latency and open times) obtained by repeated test pulse stimulation following the conditioning pulse of a particular duration was represented as

$$t_w(1), t_w(2)...t_w(i)...t_w(n) \tag{3}$$

where w and n represent the dwell state and the total number of events in the time series, respectively (*see* Fig. 8a). This unidimensional array of single-channel dwell times was used to calculate the autocorrelation coefficient (r) between the original array and the same array displaced by a lag, k. The autocorrelation function is defined as

$$r(k) = \mathrm{Cov}[t_w(i), t_w(i+k)]/(\mathrm{Var}[t_w(i)]) \tag{4}$$

where Cov and Var represent covariance and variance, whereas the dwell time and the number of lags are denoted by w and k, respectively. Covariance is defined as

$$\mathrm{Cov}[t_w(i), t_w(i+k)] = \frac{1}{n-k}\sum_{i=1}^{n-k}(t_i - \bar{t})(t_{i+k} - \bar{t}) \tag{5}$$

where $\bar{t}$ is the mean dwell time. The variance function is defined as

$$\mathrm{Var}[t_w(i)] = \frac{1}{n^2}\sum_{i=1}^{n-k}(t_i - \bar{t})^2 \tag{6}$$

The autocorrellogram was constructed by plotting the correlation coefficients against time, where time is the product of the number of lags and the duration of a sweep (one lag is equal to a sweep). The correlation coefficient can take any value between −1 and 1, where 1 represents a perfect positive correlation, −1 represents a perfect negative correlation and 0 represents random gaussian noise. Data of finite size, like channel dwell times which are subject to random variability, show a correlation coefficient close to 0; and a correlation was only considered to be significant if it was larger in absolute value than $2/\sqrt{n}$ (double the standard deviation), where the observed series is of length n (Labarca et al., 1985; Cox & Lewis, 1966).

Results

The rNav1.2α-subunit, when expressed in a heterologous system, forms a functional channel with kinetics grossly identical to the voltage-gated sodium channel in the native system though the β-subunits modulate the channel kinetics in specific ways (Majumdar & Sikdar, 2005). Figure 1a

shows representative single-Na^+ channel current traces elicited by depolarizing pulses of 10, −10 and −30 m*V*, respectively. The patch contained only one channel, showing no overlapping openings in about 1,800 traces examined. The current traces show a faster opening and shorter latency at more depolarized potentials compared to a higher number of openings and longer latency at less depolarized potentials. The single-channel slope conductance obtained from the single-channel current-voltage plot (Fig. 1b) was estimated to be 15.7 pS at 15°C, which is characteristic of voltage-gated sodium channels (Sigworth & Neher, 1980; Grant, Starmer & Strauss, 1983; Kunze et al., 1985).

First Latency Time Changes as a Function of Conditioning Pulse Duration

The first latency time, i.e., time to the first opening of the channel after the test pulse onset, represents the transition from the closed to the open state following inactivation and provides information about the recovery from inactivation of the single channel. Representative single-Na^+ channel current traces elicited by the test pulse without a conditioning pulse (control) and by 100- and 600-ms conditioning pulses (see "Materials and Methods") are shown in Figure 2a. Following a 100-ms conditioning pulse, the channel shows a tendency to open late compared to the 600-ms conditioning pulse, where the opening is quite rapid after the pulse onset. The first latency times in both cases are significantly different from the control Na^+ channel activity. Figure 2b illustrates the cumulative latency distribution histograms constructed from the activity during the test pulse following conditioning pulses ranging 0–1,200 ms from a patch containing one channel. The difference between the cumulative distribution histograms was statistically extremely significant (Kruskal-Wallis test, $p < 0.0001$, $n = 6$). The variation in the first latency observed during the test pulse application may be an experimental artifact due to repeated pulse application or due to the accumulation of slow inactivation from previous depolarizing pulses. To verify this, the latency times during the initial part of the conditioning pulse as well as the test pulse were quantified. First latency distribution histograms during the first 40 ms of the conditioning pulse (Fig. 3a, left panel) differed insignificantly from each other (Kruskal-Wallis test, $p = 0.37$, $n = 5$), whereas the latency time distributions during test pulse application (Fig. 3a, right panel) following the conditioning pulse showed

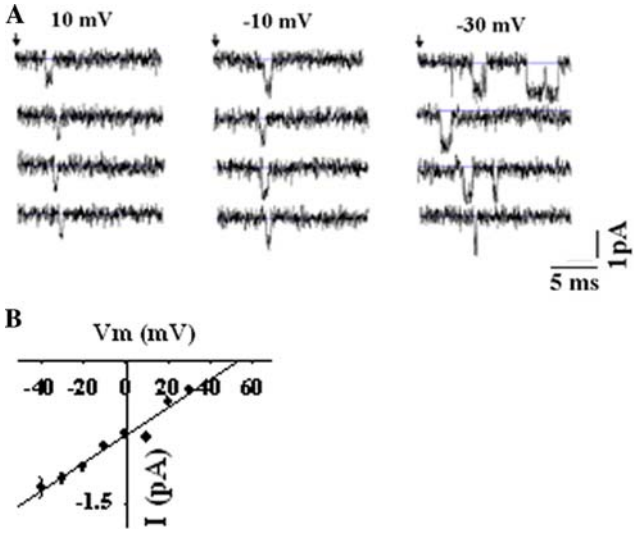

Fig. 1 Single-channel Na^+ current recorded from a cell-attached patch containing a single sodium channel from CHO cells expressing rNav1.2α-subunit. **a** Representative single-Na^+ channel current traces without digital filtering elicited by depolarizing pulses to −30, −10 and 10 m*V* from a holding potential of −90 m*V*. Pulses were applied at 0.5 Hz frequency, and the data were sampled at 50 kHz. *Small arrows* mark the onset of the pulse. Representative traces show a decrease in current amplitude with depolarization and an increase in reopening probability with hyperpolarization. All recordings were from the same patch. **b** Single-channel *I-V* relation used to estimate the single-channel slope conductance (data presented as mean ± SEM, $n = 5$–7), which was found to be 15.7 pS

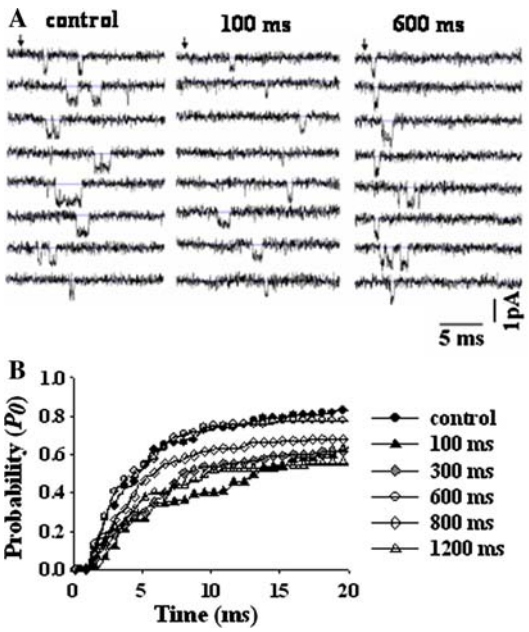

Fig. 2 Conditioning pulse durations affect single-sodium channel first latency times. **a** Single-channel current traces elicited during test pulse following conditioning pulses of varying durations. *Small arrow* marks the onset of the test pulse. After a conditioning pulse of variable duration (−10 m*V*), a test pulse of −10 m*V* was applied following a brief recovery (−90 m*V*, 80 ms). **b** Cumulative distribution histogram of first latency times following different conditioning pulse durations (0–1,200 ms) from the same patch as in **a**. Note that the asymptotic probability value, p_o, for the latency distribution changes with different conditioning pulse durations. Every third data point has been plotted for better readability

extremely significant differences (Kruskal-Wallis test, $p < 0.0001$, $n = 5$). This suggested that the variation was a result of conditioning pulse application. The observed variation can also be an artifact of stimulation frequency (0.5 Hz in our case). This was verified by analyzing the latency time distributions from data sets acquired by applying pulses at varying stimulation frequencies ranging from 0.16 to 0.5 Hz. The first latency distribution histograms (Fig. 3b, left panel) for the initial part of a conditioning pulse of 600 ms (Kruskal-Wallis test, $p = 0.778$, $n = 3$) and the corresponding test pulse (Fig. 3b, right panel) showed no significant variation (Kruskal-Wallis test, $p = 0.84$, $n = 3$) with frequency of pulse application. The solid lines in Figure 3a (right panel) illustrate the fitted exponential cdf (*see* "Materials and Methods"). With only one channel in the patch, the first latency distribution histograms were best fitted to a sum of two exponential cdfs. For patches containing more than one channel, appropriate correction was applied ("Materials and Methods"). The temporal dependence of first latency times does not seem to be linear, as illustrated in Figure 4a and b, where τ_{fast} and τ_{slow} values are plotted against conditioning pulse durations ranging 0–800 ms (data shown as mean ± SEM, $n = 6$–7). The scattered data reveal a nonlinear, rather oscillatory dependence on the conditioning pulse duration. Linear regression analysis of the data points suggests a poor fit ($R^2 = 0.04493$ and 0.0236 for τ_{fast} and τ_{slow}, respectively). Time constants τ_{fast} and τ_{slow} obtained from the fits of the first latency cdfs showed significant conditioning pulse duration-dependent variation (*see below*, Fig. 5d). The plot illustrates the percentage change in the τ_{fast} values of first latency (shown in gray bars) relative to the control condition upon different durations of conditioning depolarization (data shown as mean ± SEM, $n = 6$–7). Statistically significant variations in latency times relative to the control are especially conspicuous following conditioning pulses of 100, 400, 600 and 700 ms (Mann-Whitney test, $p = 0.002$, 0.0018, 0.01, and 0.0029, respectively).

Dependence of the Kinetic Parameters Associated with Channel Transitions on Conditioning Pulse Duration

To quantitatively describe the observed nonlinear temporal dependence of the time constants of the first latency distribution (Fig. 4a, b), wavelet analysis was performed on the data sets. Analysis of the oscillation in the experimental

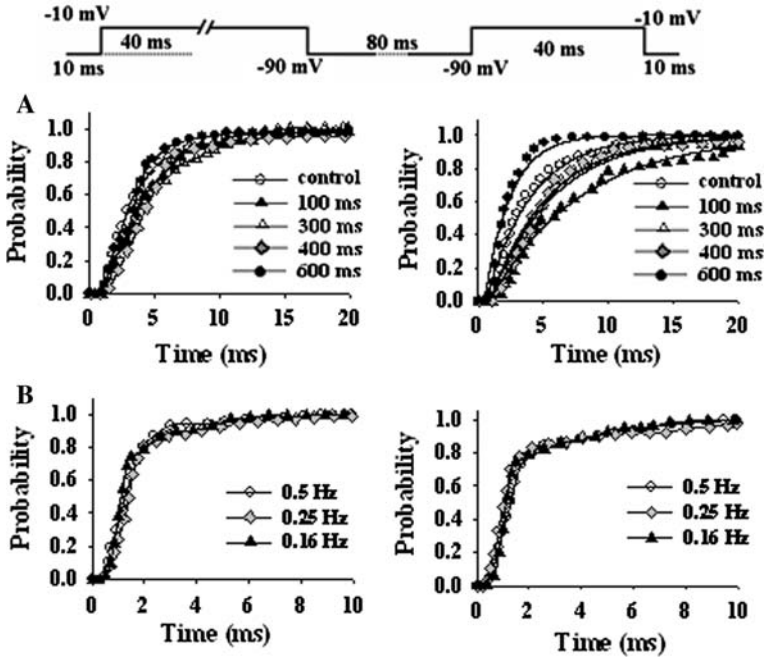

Fig. 3 First latency time is a function of the duration of conditioning pulse depolarization. **a** The pulse protocol illustrates the conditioning pulse of variable duration (shown by *broken line*), followed by a test pulse of 40-ms duration, with intervening recovery period of 80 ms. The first latency distribution histograms during control (no conditioning pulse) and the first 40 ms of conditioning pulse of durations 100, 300, 400 and 600 ms (*left panel*) differ insignificantly from each other. The latency time distribution during test pulse (*right panel*) following the above conditioning pulse durations for the same patch shows significant differences. *Solid lines in the right panel* represent the exponential cdfs fitted to the distribution histograms. **b** *Left panel* shows the first latency distribution histograms during the first 40 ms of a 600-ms conditioning depolarization with stimulation frequencies of 0.5, 0.25 and 0.16 Hz, whereas the *right panel* illustrates the first latency distribution histograms during the test pulse following a 600-ms conditioning pulse for the same stimulation frequencies. Every third data point has been plotted for better presentation

data using WWZ analysis (*see* "Materials and Methods") has its basis in the time-variant, nonstationary nature of the experimental data, where the DFT cannot be applied. Besides, FT does not resolve the component frequencies in the time domain. In contrast, wavelet analysis resolves the component frequencies and their corresponding time of occurrence. Frequencies with WWZ scores less than 1 were statistically insignificant and ignored, whereas a concentric circle in the contour plot indicates a peak for a statistically significant oscillation with WWZ score more than 1. The contour plot for τ_{fast} distribution illustrated two statistically significant oscillatory components of frequencies ~5 and ~9 Hz in the 150–650 ms range (Fig. 4a, inset). WWZ analysis revealed signatures of "pseudoperiodic" oscillations in the kinetic parameters (Majumdar et al., 2004) obtained from the analysis of first latency. The term "pseudo-oscillation" refers to an oscillation with a period that may not be the true oscillatory period since this would depend on the extent of the conditioning membrane depolarization range studied experimentally. A similar analysis performed on τ_{slow} distribution also showed significant oscillatory components in the time series (Fig. 4b, inset). The WWZ contour maps show the time-dependent variation in the oscillatory component and the time period (1/frequency) of the oscillations. Analysis of the time series by DFT (TS program, "Materials and Methods") corroborated the presence of statistically significant variable frequencies in the data, which were used to generate model curves for the scattered data by inverse FT using the TS program. The solid curve in Figure 4a and b shows the model curve generated by TS analysis, which fits the data extremely well.

Assuming that other single-channel properties like the open and close time distributions would also undergo change upon conditioning depolarization, we analyzed the open and close times as discussed in "Materials and Methods." Figure 5a shows the raw current traces following varying conditioning pulses, where the relative effect of the conditioning pulses on the first latency and open times are highlighted. Cumulative distribution histograms constructed for open times following varying durations of depolarization ranging 0–1,200 ms obtained

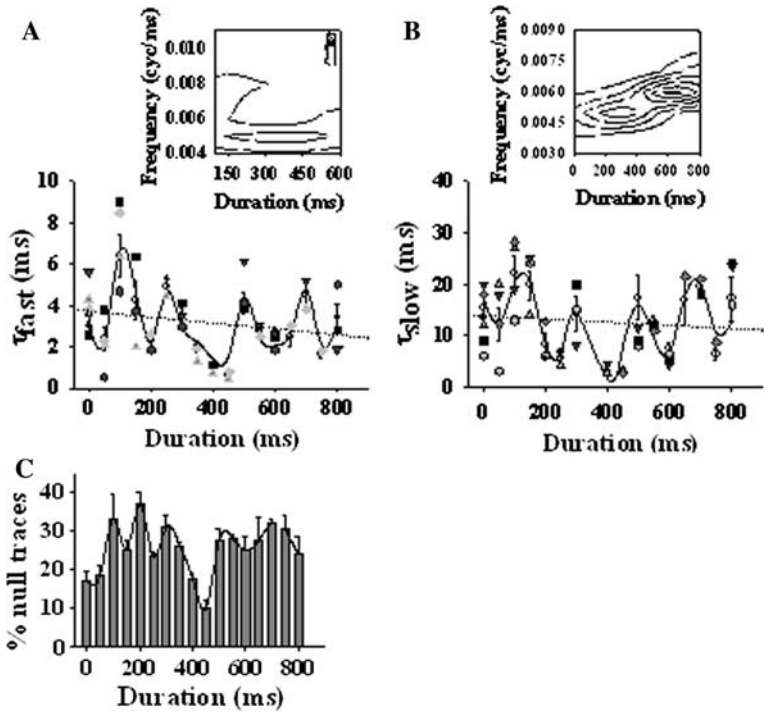

Fig. 4 Variation in the single-sodium channel kinetic parameters is nonlinear and pseudoperiodic as a function of conditioning pulse duration. **a** Variation in the fast time constant of the first latency distribution (τ_{fast}) with the conditioning pulse duration. The sampling interval was 50 ms. Different symbols represent data from different experiments ($n = 6$). *Solid curve* through the data points is the model generated by inverse FT from the component frequencies. *Dotted line* is the linear regression line ($R^2 = 0.045$). *Inset* shows the contour plot generated by the WWZ program for the fast time constant (τ_{fast}) data. The *x* axis is the conditioning pulse duration (ms), *y* axis represents the frequency (cycle/ms) and contours show significant oscillations with Z score more than 1. **b** Similar results as in **a** for the slow time constant (τ_{slow}) values. The linear regression line is shown as a *dotted line* ($R^2 = 0.023$) indicating a poor fit. **c** Plot of percentage null traces *vs.* conditioning pulse duration, which depicts the nonlinearity in close to inactivation transition. The percentage null traces are presented as the mean ± SEM obtained by pooling data from many patches ($n = 8$). *Solid curve* passing through the mean values shows the nonlinearity in the data

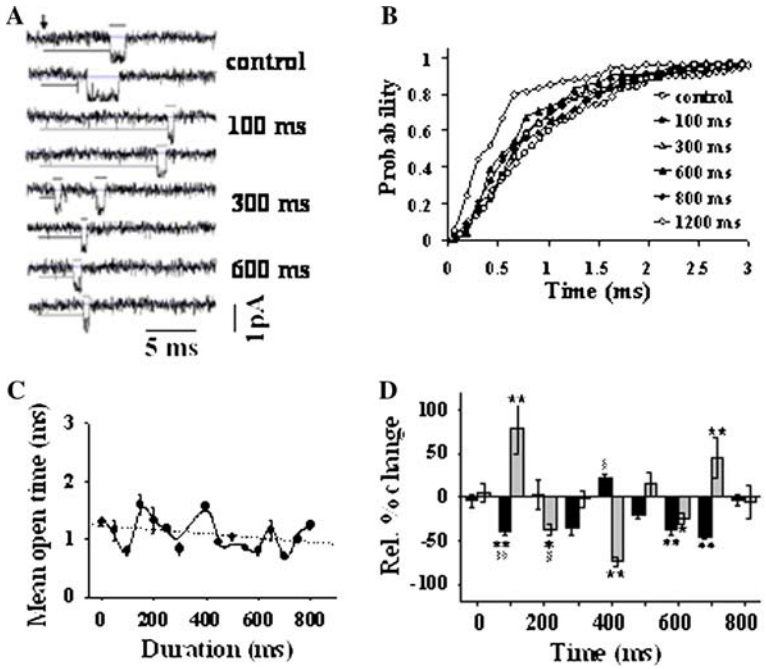

Fig. 5 Single-channel open times vary nonlinearly with conditioning pulses of varying duration. **a** Single-Na^+ channel current traces following varying conditioning pulses (duration indicated) highlight the open dwell times and first latency times. **b** Cumulative distribution histograms of the open times following varying conditioning pulses for the same patch as in Figure 2b. **c** Plot of mean open times following varying conditioning pulses. *Solid line* passing through the data points is the TS model that fits the data. *Dotted line* shows the result of linear regression analysis of the data points (R^2 = 0.10) indicating a poor fit. **d** Relative percentage change (mean ± SEM) in the mean open time (*black bars*) and τ_{fast} of first latency times (*gray bars*) following varying durations of conditioning pulse with respect to the control condition (no conditioning pulse). The symbols '·', '⇐' and § illustrate statistically significant differences (Mann-Whitney test; '·', '*' and §, $p = 0.05 \leq p \leq 0.01$; '··','**'and '§§' $p = 0.001 \leq p \leq 0.01$) in case of first latency and open times and between open and first latency times, respectively, following a conditioning pulse

from the same patch as in Figure 2b were observed to be significantly different (Kruskal-Wallis statistical test, $p < 0.005$, $n = 9$) (Fig. 5b). The open time distribution for patches containing only one channel was best fitted to a monoexponential function. The distribution of mean open times with the conditioning pulse duration was nonlinear, which was verified to be of pseudo-oscillatory nature by WWZ and TS analyses of the data (n = 6–8) (Fig. 5c). A linear regression analysis (dotted line, Fig. 5c) further supported the nonlinear nature of the data owing to a poor fit of the regression line (R^2 = 0.103). The relative percentage change in the mean open times (black bars) following varying conditioning pulse durations with respect to control was estimated and presented as mean ± SEM (n = 6–7). It showed significant variation in mean open times with the conditioning pulse duration (Fig. 5d). The variation is particularly significant following 100, 300, 600 and 700 ms pulse durations (Mann-Whitney test, $p = 0.008$, 0.022, 0.01 and 0.004, respectively). Both the mean open times and τ_{fast} of latency times undergo significant changes upon sustained depolarization. This was inferred from the paired comparison of the relative changes in mean open times and τ_{fast} of latency times, which showed insignificant variations. The exceptions to this were observed at the 100- and 200-ms conditioning pulses (Mann-Whitney test, p = 0.0079 and 0.0286, respectively). Similar analysis done for the close time distribution (*data not shown*) confirmed that the nonlinear nature is inherent to all kinetic parameters associated with channel transitions.

Voltage-gated sodium channels are known to undergo transition from the closed to the inactivated state(s). Such transitions are indicated by traces with no channel activity during the test pulse (null traces). The percentage of null traces following different conditioning pulse durations was estimated and plotted as a bar diagram (Fig. 4c). The data (mean ± SEM, $n = 8$) depict a nonlinear relationship between the fraction of null traces and the conditioning pulse duration. This is also evident from Figure 2b, where the asymptotic probability (p_o) of the first latency distribution is less than 1 and shows the dependence of close to inactivation transition on the conditioning pulse duration. Asymptotic values less than 1 reflect the fraction of channels that pass directly to the inactivated state without opening (Aldrich et al., 1983).

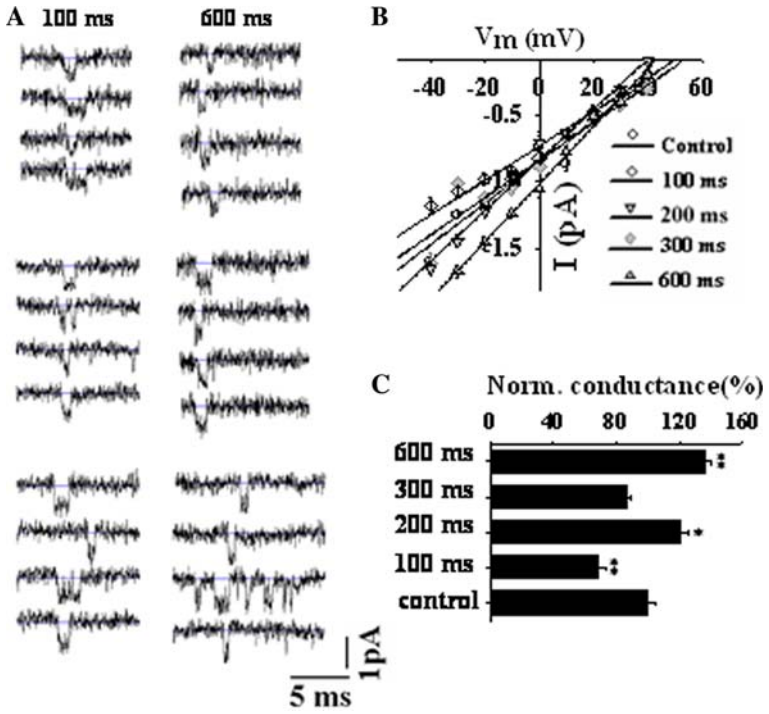

Fig. 6 Conditioning pulse duration affects single-sodium channel conductance. a Single-channel current traces at test potentials (10, −10, −30 m*V*) with 100-ms (*left panel*) and 600-ms (*right panel*) conditioning depolarization pulses. Note the differences in single-channel current amplitudes following the conditioning pulses. **b** Single-channel *I-V* relation following different durations of conditioning depolarization ranging 0–600 ms. The slope conductance was obtained by passing a linear regression line through the mean single-channel current amplitudes (*solid line*). The slope conductance and the R^2 for the linear regression fits are 15.7 pS, 0.90 (control); 10.9 pS, 0.95 (100 ms); 18.66 pS, 0.87 (200 ms); 13.52 pS, 0.95 (300 ms); and 21.06 pS, 0.97 (600 ms), respectively. **c** Percentage change in Na^+ channel unitary conductance following varying conditioning pulses with respect to the control condition (no conditioning pulse). The unitary conductance of the Na^+ channel changes as much as ±30% of the control condition following varying conditioning pulses. Statistically significant variations (Mann-Whitney test) are indicated adjacent to the bars in the histogram (*$p = 0.05 \leq p \leq 0.01$, **$p = 0.001 \leq p \leq 0.01$)

Single-Channel Slope Conductance Changes with Varying Conditioning Pulse Durations

The pronounced changes in the above kinetic parameters of single sodium channels following conditioning pulses of varying durations were also accompanied by a significant change in the unitary current amplitude. This is illustrated in Figures 2a and 6a, where the measured current amplitudes at –10 m*V* upon 600-ms conditioning depolarization are larger than the current amplitudes following 100-ms conditioning pulse. These differences suggested possible changes in single-channel conductance. The single-channel conductance was estimated from the slope of the single-channel *I-V* relationship. With increased conditioning pulse duration, the single-channel conductance was expected to decrease since the molecule would be in a slow inactivated state(s) (Toib et al., 1998). In contrast, the single-channel conductance without a conditioning pulse was 15.7 pS, while with conditioning pulse durations of 100, 200, 300 and 600 ms, the single-channel conductances were 10.9, 18.66, 13.52 and 21.06 pS, respectively (Fig. 6b). The slopes of the single-channel current-voltage relationship were significantly different ($p < 0.0001$ at 95% confidence level, $n = 5$). The change in conductance following varying conditioning pulses is presented as the percent change with respect to the control condition (no conditioning pulse) (Fig. 6c). It shows a change of ±30% in the conductance values following varying durations of conditioning depolarization of the single Na^+ channel. The relative changes are statistically significant with reference to the control (Mann-Whitney test, $p = 0.001$, 0.021 and 0.0012, respectively, for 100, 200 and 600 ms). A nonlinear relationship between the single-channel conductance and conditioning pulse duration is clearly evident from these data, similar to that observed for other kinetic parameters. This suggests a possible correlation between unitary conductance and the dwell times of single channels. In order to explore this possibility, the observed mean latency times and the corresponding conductance values for various conditioning pulses were plotted as a 2D scatter (Fig. 8b). This clearly showed an inverse correlation between the unitary conductance and first latency of the single Na^+ channel. A decaying monoexponential function fits the data well, confirming the inverse relationship ($R^2 = 0.79$), shown in Figure 8b (dotted line). Though a similar relationship was observed earlier between adjacent open and

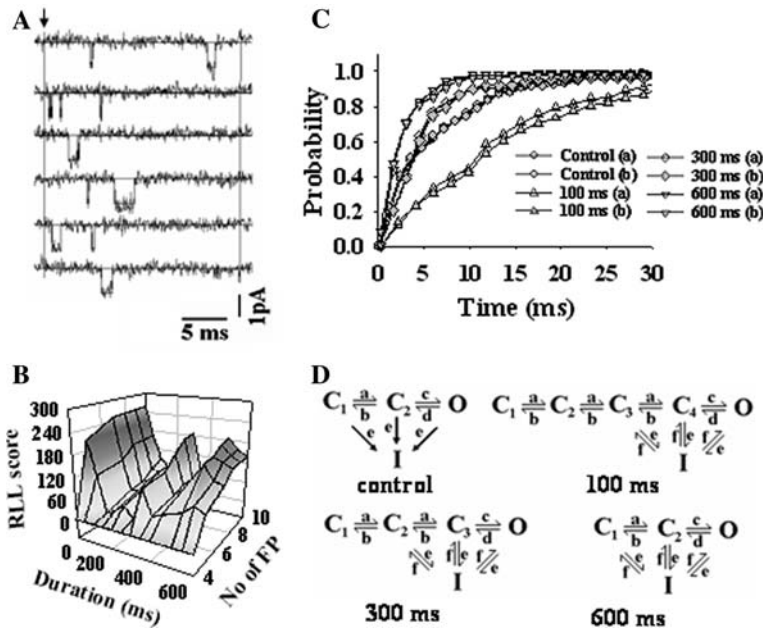

Fig. 7 RLL values generated by HMM models with increasing complexity for a single sodium channel vary with conditioning pulse duration. **a** Leak-subtracted single-sodium channel current traces used for HMM. *Vertical lines* show the selection window used for analysis (40 ms). *Arrow* marks the onset of the pulse. *Solid lines* show the model generated by HMM to fit the single-channel current trace. **b** 3D plot showing the variation in the complexity of the model that best described the single-channel current activity at different conditioning pulses. The *x* axis shows the number of free parameters (*FP*) of the HMM (*see* Table 1), *y* axis shows the conditioning pulse duration and *z* axis shows the RLL scores obtained from HMM. **c** Comparison of cumulative distribution histograms obtained by half-amplitude threshold crossing method (*a, open symbols*) and those estimated from the modeled single-channel events using HMM analysis (*b, filled symbols*) following varying conditioning pulses (control and 100, 300 and 600 ms). Every fourth data point is plotted for better readability. **d** Best models (*C*, closed; *O*, open; *I*, inactivated state) obtained by HMM following varying depolarizing pulses (indicated below models). *Small letters* refer to the transition rate constants of the respective models (Table 1), which were estimated and are presented in Table 2

shut intervals for Cl^- and K^+ channels (McManus, Blatz & Magleby, 1985), the induction of an inverse correlation between conductance and first latency owing to conditioning pulse depolarization has not been reported earlier.

Underlying State Sequences Associated with Na^+ Channel Gating Change with Varying Conditioning Pulse Durations

In order to verify whether the varying depolarization pulses were indeed causing dynamic changes in the sodium channel kinetics and the underlying state transitions, we used a more direct approach for data analysis, which consisted of directly fitting the HMM to the raw single-channel current data (Fig. 7a, *see* "Materials and Methods"). The inverse filtered raw current traces were used for the HMM as discussed in "Materials and Methods." The basic model comprised three states – closed, open and inactivation (Aldrich et al., 1983) – and the complexity of the model varied by including additional states and transition rate constants. A maximum likelihood method was used to fit the HMM models to raw data. The log likelihood (LL) scores obtained for ten different models were compared relative to the basic model. A model was adjudged better over a lower complexity model only if it registered a rise in RLL score by $\sim$10 units per free parameter (Zheng et al., 2001). The HMM results are tabulated in Tables 1 and 2. Comparison of the RLL scores generated by models with increasing complexity (Fig. 7b) shows that with a 100-ms conditioning pulse a model with more closed states best described the data (model X). For a five-state model (model VII), there was a rise of 26 log units over a four-state model (model V). With one more closed state, the LL score rose by 22 units and, hence, was regarded as the best fit to the data. On the contrary, the single sodium channel current elicited following a 600-ms depolarization was best described by the four-state model (model V, rise of 135 log units for four parameters), showing no betterment in the RLL scores with increasing number of free parameters. The results clearly show a nonlinear change in the preference for the type of model and number of states over the range of conditioning pulse durations tested (Fig. 7d). The increased

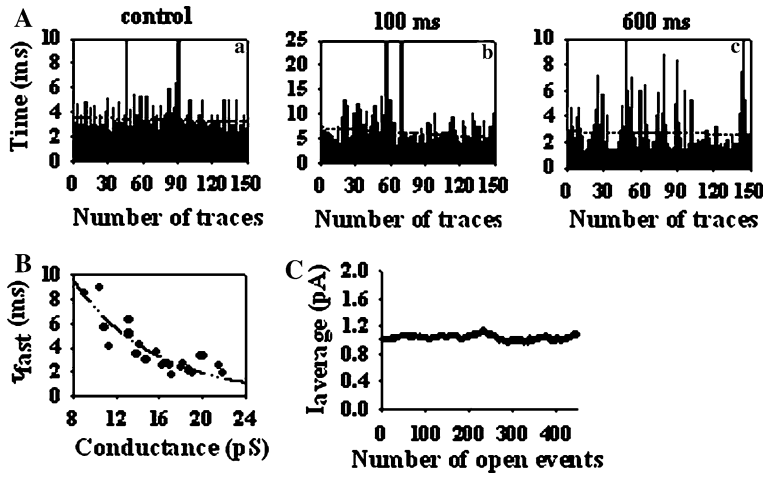

Fig. 8 Single-channel activity of voltage-gated sodium channel becomes ordered following conditioning depolarization. **a** Plot of the first latency times for each of the traces during the test pulse following conditioning pulses of 0, 100 and 600 ms against the trace number for a patch containing one channel. *Dotted lines* show the linear regression of the latency time series data with *y* intercepts (slopes) 3.5762 (−0.0024), 7.212 (−0.0132) and 2.182 (−0.0014) for 0, 100 and 600 ms conditioning pulse durations, respectively. Note the appearance of orderliness in the data with increasing duration of conditioning depolarization. **b** 2D scatterplot of the τ_{fast} of the first latency times against the corresponding slope conductance of the channel following varying conditioning pulses. Note that τ_{fast} was estimated from the analysis of first latency times during the test pulse of −10 m*V*. The data shown here were obtained from several experiments (n = 6). *Dotted line* is the fit with a decaying monoexponential function (R^2 = 0.79). **c** Stability plot for one of the data sets shown in Figure 2, obtained by plotting the moving average of current amplitudes (pA) of 50 successive open events on the *y* axis against the number of open events on the *x* axis

number of states required to describe the channel activity following a 100-ms conditioning pulse depolarization corroborates the long latency times observed earlier (Fig. 2a). Table 2 illustrates the transition rate constants (s^{-1}) resulting from the HMM for the best models (highlighted in bold in Table 1) describing the data following particular conditioning pulses. As per the RLL scores, data following 50-, 200-, 400-, 550- and 600-ms conditioning pulses are best explained by models V and IV (four-state models), whereas data following 100, 250 and 500 ms are described by a six-state model (model X). A comparison of transition rate constants for above two categories of data showed that with increasing duration of conditioning depolarization the C_x-C_y (transition between closed substates) transition rate increased linearly whereas the C-O (closed to open) transitions remaining approximately constant throughout. This has been highlighted in Table 2 (black for four-state models and gray for six-state models). It can be inferred from this observation that at longer depolarization a closed-closed transition is comparatively more probable than a closed-open transition; thus, a closed state is more likely succeeded by a closed state than an open state, leading to clustering of events. It can be observed from Table 2 that the C_x-C_y and C-O transitions in a six-state model are much slower compared to a four-state model, thus explaining the longer latency times observed from the half-amplitude threshold crossing method. The I-C_x (inactivation-closed) transition rates, however, in all the conditions are slow, which suggests a small reopening probability of the Na^+ channel studied. HMM analysis has been used as a complementary approach along with dwell time analysis. The results obtained by HMM analysis comply with those obtained by the half-amplitude threshold crossing method. This has been shown (Fig. 7c) as a comparison of cumulative distribution histograms obtained from the half-amplitude threshold crossing method (open symbols, a) and HMM analysis (filled symbols, b) following varying durations of conditioning depolarization (control and 100, 300 and 600 ms). The difference between the pairs in all the above cases was statistically insignificant. Hence, HMM analysis was a faithful tool in determining the kinetic parameters and drawing an appropriate kinetic scheme of the channel upon conditioning depolarization.

Molecular Memory Phenomenon in a Single Voltage-Gated Na^+ Channel

Statistical analysis of dwell times, single-channel conductance and HMM of kinetic state transitions substantiate the induction of a defined nonlinear change (pseudo-oscillatory) in channel properties by the conditioning depolarization. It is expected, therefore, that the activity of the channel would show nonrandom temporal behavior with repeated membrane depolarization by a conditioning pulse paired with the test pulse. To explore this possibility, we performed autocorrelation analysis on channel dwell times. The series of first latency times (for the data shown

Table 1 HMM analysis results for single sodium channel

Model No.	Models	Free Param.	Conditioning pulse duration (ms)											
			00	50	100	150	200	250	300	350	400	500	550	600
I	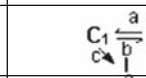	4	0	0	0	0	0	0	0	0	0	0	0	0
II	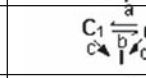	5	194	108	2	21	16	9	98	18	36	5	76	48
III	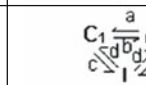	5	207	113	8	23	44	13	104	34	46	66	89	73
IV	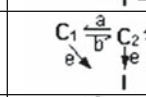	7	**248**	124	37	42	65	33	112	49	**73**	152	114	106
V	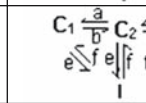	8	251	**159**	40	57	**83**	36	148	**61**	76	159	**148**	**135**
VI	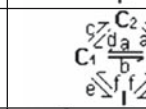	8	226	119	15	39	48	26	103	40	67	78	96	78
VII	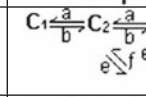	9	253	160	66	**64**	86	38	**180**	64	77	178	152	136
VIII	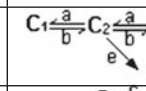	9	251	147	72	48	74	33	166	52	73	173	138	110
IX	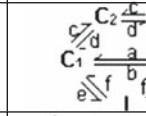	9	249	121	19	46	54	29	114	48	64	86	104	80
X	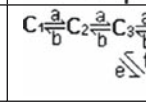	10	255	162	**88**	68	88	**56**	185	64	78	**186**	155	136

HMM analysis validates the variation in underlying state transitions following different conditioning pulse durations. The table shows the RLL scores obtained by HMM analysis with different models (I-X). In all, ten models were used for the analysis, and the scores are presented relative to the first (nested) model. Scores in bold represent the best score and suggest the best model for a particular conditioning pulse duration. Gray- and black-labeled conditioning pulse durations suggest that similar models best describe the corresponding single-channel data (gray by four-state model and black by six-state model)

in Fig. 2b) during the test pulse following conditioning pulses of 0, 100 and 600 ms are plotted against the respective times of occurrence (trace number) and illustrated in Figure 8a. The intercept of the linear regression line with the ordinate shows the mean latency times, which is in agreement with the value obtained from the half-amplitude threshold method. Visual inspection of the experimental data shows a distinct clustering of data in latency time series; i.e., a longer latency is more likely followed by a longer latency than a shorter one in case of longer depolarization for, e.g., the 600-ms conditioning pulse in contrast to the control, where the data are more randomly distributed (Fig. 8a). With a 100-ms conditioning pulse, the clustering is intermediate between control and the 600-ms conditioning pulse (Fig. 8a). This prompted us to do the autocorrelation analysis on the data obtained during the test pulse and the initial part of the conditioning pulse. Figure 9a illustrates the autocorrellograms for the series of first latency data obtained for control (no conditioning pulse, a) and during the initial part of conditioning pulses of durations 100 (b) and 600 (c) ms. The autocorrelation function, in all the above cases, seems to be insignificantly different from zero, suggesting the absence of any correlation in the data. This further corroborates our finding that the latency times do not vary significantly in the initial part of the conditioning pulse (Fig. 3a). On the other hand, similar analysis of the test pulse data following the conditioning pulses showed significant correlation in

Table 2 State transition rate constants for best models of HMM analysis

Transitions (s^{-1})	Conditioning pulse duration (ms)											
	00	**50**	**100**	**150**	**200**	**250**	**300**	**350**	**400**	**500**	**550**	**600**
C_1-C_2	423	622	169	852	770	242	482	196	996	302	1270	2040
C_1-I	48.1	473			582			116	739		247	276
C_2-C_1	1510	212	456	254	59.7	540	282	818	1160	654	139	0
C_2-C_3			227	393		316	562			530		
C_2-O	**2910**	**4530**			**3820**			**1630**	**4130**		**1240**	**3790**
C_2-I	421	113		1420	224	132	295	298	34.3		807	247
C_3-C_2			407	49.6		276	174			54		
C_3-C_4			696			712				952		
C_3-O				**5560**			**3040**					
C_3-I			1070	378		619	649			334		
C_4-C_3			38.5			104				153		
C_4-O			**276**			**248**				**396**		
C_4-I			305			295				15.8		
O-C_2	383	285			224			187	196		137	124
O-C_3				132			97.2					
O-C_4			203			327				124		
O-I	448	508	542	323	434		857	891	372	136	1070	664
I-C_1	*1.4*	*35.4*			*5.24*			*8.31*	*0*		*9.15*	*9.32*
I-C_2	*0.52*	*3.44*		*12.1*	*22.4*		*3.36*	*9.66*	*0*		*5.28*	*0.39*
I-C_3			*12.1*	*3.07*		*22.5*	*9.09*			*1.12*		
I-C_4			*2.4*			*0.94*				*9.06*		
I-O	*0.37*	*0.054*	*10.7*	*0*	*20.1*	*0*	*0.39*	*0.56*	*0*	*0.845*	*1.88*	*0.055*

Transition rate constants (s^{-1}) obtained from HMM analysis for the best models, highlighted in bold in Table 1. The rate constants of the state transitions not associated with the best models have been suitably omitted. The symbols C, O and I represent the closed, open and inactivation states, respectively. The conditioning pulse durations highlighted in black and gray belong to two groups, where the data were best described by two different models (black by four-state and gray by six-state model). Black- and gray-highlighted transition rate constants illustrate transition rates of significance (see "Results"). Italicized rate constants represent the slowness of the inactivation-closed and inactivation-open transitions

the data (Fig. 9b, left panel). The control data series in Figure 9b(a) seems to be devoid of any correlation with values of correlation coefficients close to zero. The data series following a 100-ms (Fig. 9b[b]) conditioning pulse shows a strong correlation for the initial few lags ($\sim$30), persisting up to less than 100 s, after which the correlation is not significantly different from zero, whereas following a 600-ms pulse the data series (Fig 9b[c]) shows an extremely significant correlation ($r > 0.24$) up to $\sim$300 s (>100 lags). The number of data points is similar in all the above cases. In order to negate the possibility that the observed correlation can be an artifact of the analysis, we randomized the data series and recalculated the correlation. The right panel in Figure 9b shows the autocorrellograms of the randomized data for the corresponding data sets in the left panel. It shows the absence of correlation in the randomized data. Autocorrelation analysis was performed for data sets of different conditioning pulses, and conditioning pulse duration dependence of autocorrelation was clearly observed in all cases. The above results imply that statistically significant correlation is induced in the time series by the conditioning depolarization, which persists for longer periods with progressively longer duration of conditioning pulses. Another striking feature of the autocorrellograms is that the decay of correlation functions is not monotonous but shows fast oscillations. As there is no evidence of any autocorrelation or oscillations in the initial part of the conditioning pulse, we suggest that the origin of correlation as well as the fast oscillation are due to the conditioning pulses. Identical results were observed for at least six different patches. Similar analyses on the open times also showed induction of significant depolarization duration-dependent autocorrelation in the data series (*data not shown*). These results illustrate the role of sustained membrane depolarization in altering channel kinetic properties in a defined nonlinear manner and inducing a molecular memory phenomenon of the previous activity.

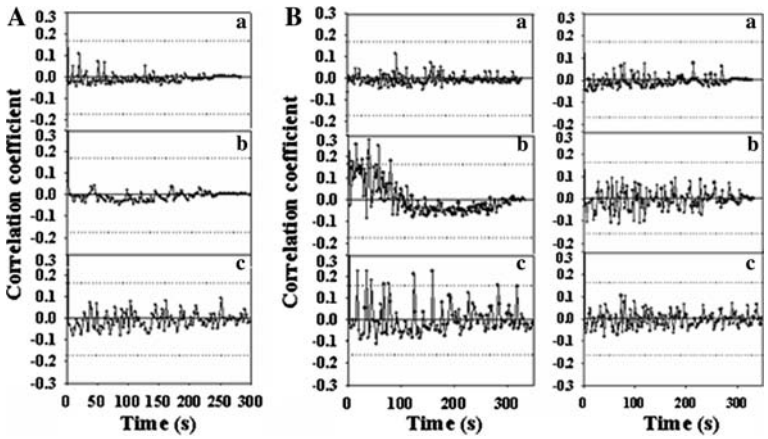

Fig. 9 Autocorrelation analysis suggests the presence of a molecular memory phenomenon in single sodium channel. **a** Autocorrellograms for the series of first latency time data obtained during the first 40 ms of the conditioning pulse for the same patch as in Figure 8a. Shown here are the autocorrellograms obtained for control (0 ms conditioning pulse, *a*) and conditioning pulses of 100 ms (*b*) and 600 ms (*c*), where the *x* axis is the time (s) and the *y* axis shows the correlation coefficient. Note that the number of lags (*k*) has been appropriately transformed into time (s) by incorporating the time between the end of the first latency time measurement and the beginning of the next test pulse in the sequence. *Solid straight line* indicates 0 correlation, whereas *dotted line* indicates significant correlation ($2/\sqrt{n}$, *see* "Materials and Methods"). **b** Autocorrellograms of the first latency times obtained during the test pulse following conditioning pulses of 0 (control, *a*), 100 (*b*) and 600 (*c*) ms (*left panel*) for the same patch as in **a**. *Right panel* illustrates autocorrellograms of the corresponding data in *left panel*, where the time series has been randomized by a random number generator algorithm. The *x* and *y* axes represent time (s) and correlation coefficient, respectively, whereas the *solid* and *dotted lines* here have the same meaning as in **a**

Discussion

The present study reports a novel nonlinear property of the single voltage-gated sodium channel. Our results suggest that voltage-gated sodium channels exhibit a molecular memory phenomenon induced by conditioning depolarization. The rNav1.2α-subunit heterologously expressed in CHO cells is an appropriate system for studying single-voltage-gated sodium channel properties. The single-Na^+ channel properties of the rNav1.2α, reported here, are in agreement with previous reports on the rat brain cortical neuron Na^+ channel (Kirsch et al., 1989) and the Na^+ channel expressed in neuroblastoma cell lines (Aldrich et al., 1983; Aldrich & Stevens, 1987; Ma et al., 1994). There are no reports regarding the gain or loss of function of sodium channels expressed in CHO cells. Further, the rNav1.2 channels are orthologous to the *SCN IIA* gene product of humans and share up to 80% similarity with some subtypes of human sodium channels (Ahmed et al., 1992).

In order to understand the effect of sustained depolarization, statistical analysis of channel dwell times was performed. To avoid the missed event problem in dwell time analysis, the first bin (0.08–0.16 ms) equaling the system dead time (80 μs) was always ignored ("Materials and Methods"). Dwell time analysis illustrates a significant nonlinear variation in the first latency, open and close time distributions following varying durations of conditioning depolarization. The variation, which was apparent in the test pulse data, was statistically insignificant in the initial part of the conditioning pulse (Fig. 3a). As the intertrial interval (2s) and the time allowed between successive experiments were sufficient to prevent accumulation of slow inactivation in the molecule (Fig. 3b), it is more likely that the above phenomenon is a result of conditioning depolarization alone. Studies on voltage-gated Na^+ channels subjected to prolonged depolarization in the range used in our experiments (0–1,200 ms) suggest that recovery of the channel from slow inactivation is faster than the intertrial interval of 2 s (Nuss et al., 1996; Chen et al, 2006). The lack of significant correlation in the first latency data obtained in control condition (no conditioning pulse) as well as in the initial part of conditioning pulse and the occurrence of a very significant depolarization duration-dependent autocorrelation in the test pulse data (Fig. 9b) further corroborate the above inference. The role of second messengers or any other intracellular factors in this observation is less likely, keeping in mind the time scale (a few milliseconds) in which the phenomenon was observed. The nonlinear behavior of the channel remains undiminished in excised inside-out patches (*data not shown*), which suggests that the nonlinearity is a channel property rather than a cellular one. The observed nonlinearity in the channel properties was qualified by FT and WWZ analyses to be a pseudoperiodic oscillation and could not adequately be described by linear regression fit (Figs. 4, 5). Further, the relative percentage change in the time constant values (Fig. 5d) due to conditioning depolarization, especially at

the crests and troughs of the oscillation, are significantly different, which reiterates its oscillatory nature. Similar phenomena have been observed earlier for rNav1.2α at the whole-cell level (Majumdar et al., 2004; Majumdar & Sikdar, 2005) and for bursting voltage-gated K^+ channel in fused synaptosomes from the *Torpedo* electric organ (Rahamimoff et al., 1995).

Explanation of the Nonlinearity in Channel Kinetic Parameters and Change in Conductance Lies in the Channel Conformation

The slope conductance of the single voltage-gated Na^+ channel showed significant variation relative to control conditions with varying durations of conditioning depolarization. This suggests a possible change in channel conformation induced by conditioning depolarization in and around the pore region. HMM of the raw current traces illustrates a change in the preference for different kinetic models and transition rate constants following varying durations of activity, suggesting subtle changes in underlying state sequences and state transitions in the molecule. The inverse correlation observed between first latency times and unitary conductance points to a possible coupling between the activation and recovery from inactivation processes. The sodium channel exhibits at least two major types of inactivation processes, fast and slow. Fast inactivation in voltage-gated sodium channels occurs by a "hinged lid" mechanism in which the cytoplasmic linker between domains III and IV occludes the pore of the channel (Goldin, 2003), whereas slow inactivation is a result of drastic conformational change in the channel molecule in various domains such as the pore region of domain III (Ong et al., 2000), S4 of domain IV (Miyamato et al., 2001) and S5-S6 of domain II (Vilin, Fujimoto & Ruben, 2001). There is a strong coupling between the three processes, i.e., activation, fast inactivation and slow inactivation, through the S4 helix of domain IV of the sodium channel (Goldin, 2003; Miyamato et al., 2001; Rohl et al., 1999). Continuous molecular rearrangements in the structural components of the Na^+ channel may take place during the conditioning pulse due to slow inactivation, and this may involve dynamic changes in noncovalent interactions in the molecule as well as between the inactivation lid and the docking site in the Na^+ channel (Majumdar et al., 2004). Complex voltage-dependent gating rearrangements that extend beyond the membrane-spanning channel core to the intracellular tetramerization domain, T1, have been recently reported in K^+ channels (Wang & Covarrubias, 2006). Therefore, the functional oscillation observed in our case can be a result of conformational oscillation (Vlad et al., 2002), which suggests that the various domains of the molecule may flicker several times before undergoing an open state transition. The situation could be similar to the fast open channel block, where the single-channel conductance flickers between the two states, closed and open; but since the occurrence is very rapid, the current amplitudes are blunted or reduced in amplitude by the bandwidth of the patch-clamp amplifier. This is reflected as a decrease in conductance (Hille, 2001). On the other hand, the variation in first latency times following varying conditioning pulses was due to altered channel conformations, which was established by HMM analysis (Fig. 6b, d). The observed first latency times were reflections of the rates of C-C and C-O transitions (Table 2). The temporal change in transition rate constants can be due to internal fluctuations in channel conformation due to slow inactivation extending to various channel domains. Since the slow inactivation property of sodium channels is sensitive to change even in a single amino acid residue (O'Reilly, Wang & Wang, 2001), fast and drastic dynamic changes in channel conformation are expected during the conditioning depolarization. Though experimentally the 80 ms recovery time between the conditioning pulse and test pulse was to allow the channel to recover completely from fast inactivation (as observed for whole-cell current [Majumdar et al., 2004]), we cannot rule out the possible participation of fast inactivation in conformational changes of the channel discussed above. In a nutshell, the observed nonlinear property in voltage-gated Na^+ channels following sustained depolarization is a possible outcome of the drastic conformational change due to coupling of activation and inactivation processes.

Molecular Memory in Voltage-Gated Sodium Channel and Implications in Signal Processing

Single-ion channel current traces contain important information regarding temporal correlations between channel dwell times, which is not obtainable from whole-cell current data. A series of single-ion channel responses to identical test pulse depolarization alone and a pair of conditioning pulse and test pulse with varying conditioning pulse durations was collected. Time series analysis of the experimental data consisting of first latency times (shown in Fig. 8a) and open times using the autocorrelation function (Fig. 9) suggested that the autocorrelation function is close to zero following stimulation with the test pulse alone or in the initial part of the conditioning pulse. In other words, the activity of the channel is not correlated temporally. However, this was not the case when the first latency times during the test pulse were analyzed in the conditioning pulse-test pulse pair. Adjacent first latency times were highly correlated (Fig. 8a) when the test pulse

was preceded by long conditioning pulses. Also, the autocorrellograms exhibited periodic oscillations that were sustained for variable periods before decaying to zero (Fig. 9b, left panel). The results suggest that the conditioning depolarization is the cause of the oscillations in the activity of the single-channel molecule such that a longer dwell time is followed more likely by a longer one and vice versa. Differences in the autocorrellograms observed with different conditioning pulse durations suggest that the activity of the channel is closely linked to the conditioning pulse duration. In essence, a molecular memory phenomenon arises in the channel molecule characterized by clustered dwell times and strongly correlated activity upon sustained membrane depolarization. Hence, the channel remembers the perturbation in the channel conformation induced by the previous activity. The kinetic rate constants obtained from the HMM analysis further confirm the above phenomenon (Table 2). The relatively faster C_x-C_y transition rate constant values compared to the C-O rates at longer depolarization provide a possible explanation for the observed correlation in the dwell times and, thus for the time-dependent molecular memory observed in the channel. The molecular memory mechanism operating in the voltage-gated Na^+ channel is not surprising if compared with similar observations in enzyme catalyzed reactions. Single-enzyme molecule studies have demonstrated the existence of a strong autocorrelation function of the fluorescence waiting times related to the substrate-enzyme reaction kinetics, similar to what is shown in Figures 8 and 9. Signatures of strong autocorrelation in enzyme catalyzed reactions are dependent on substrate concentration and have been associated with a molecular memory phenomenon (Vlad et al., 2002; English et al., 2005), which is analogous to the long conditioning pulse durations in the case of the voltage-gated Na^+ channels reported here. The decay in autocorrelation function seems to be closely related to the conditioning pulse duration: the longer the depolarization, the longer the persistence of the molecular memory (Fig. 9b, left panel). This may have a strong implication in neuronal signal processing and pathological conditions like epilepsy. The pseudo-oscillatory nature of the channel kinetic properties and varying unitary conductance with the duration of the conditioning pulse would imply a nonlinear voltage response of the membrane to current injections, and the molecular memory would ensure the persistence of the behavior for a stipulated amount of time. The observed molecular memory in Na^+ channel in conjunction with the observed nonlinearity in kinetic parameters may explain the intrinsic plasticity of neurons. The small variations in kinetics and conductance summed over a large number of channels can result in relatively huge changes in membrane potentials that can manifest as subthreshold or suprathreshold membrane potential oscillations. Voltage-gated Na^+ channels have been implicated in subthreshold membrane oscillations (Sanhueza & Bacigalupo, 2005), and a possible explanation is the pseudoperiodic oscillatory properties described above. Such membrane oscillations may be further exacerbated to manifest as increased membrane potential fluctuations in conditions such as epilepsy (Lian, Shuai & Durand, 2004).

Another important implication of the memory effect and pseudoperiodicity in Na^+ channel properties is in signal coding and decoding in the neurons of the central nervous system. The sodium channel Nav1.2 is abundantly expressed in the adult brain. The nonlinearity of the Na^+ channel kinetics and the memory thereof would be an appropriate mechanism that can be utilized by the neurons to finely modulate the incoming signals, especially in conditions of intense activity in neural networks and hyperexcitability. Cast within the framework of the Hodgkin-Huxley formalism classically used to describe the sodium current waveform, one might consider that the memory in the present value of sodium conductance (g_{Na}) is dependent on the previous values of the activation and inactivation variables. If these change dynamically and nonlinearly with increase in duration of the conditioning depolarization, one might expect the memory phenomenon in the single sodium channel properties that we have reported here.

Acknowledgement This work was supported by the Department of Science and Technology, India. We thank Prof. F. J. Sigworth (Yale University, New Haven, CT) for discussions and suggestions.

References

Ahmed CM, Ware DH, Lee SC, Pattern CD, Ferrer-Montiel AV, Schinder AF, McPherson JD, Wagner CB, Wasmith JJ, Evans GA (1992) Primary structure, chromosomal localization and functional expression of voltage-gated sodium channel from human brain. Proc Natl Acad Sci USA 89:8220–8224

Aldrich RW, Corey DP, Stevens CF (1983) A reinterpretation of sodium channel gating based on single-channel recording. Nature 306:437–441

Aldrich RW, Stevens CF (1987) Voltage-dependent gating of single sodium channels from mammalian neuroblastoma cells. J Neurosci 7:418–431

Amir R, Liu C, Kocsis JD, Devor M (2002) Oscillatory mechanism in primary sensory neurons. Brain 125:421–435

Berman MF, Camardo JS, Robinson RB, Siegelbaum SA (1989) Single sodium channels from canine ventricular myocytes: voltage dependence and relative rates of activation and inactivation. J Physiol 415:503–531

Chen K, Aradi I, Thon N, Eghbal-Ahmadi M, Baram TZ, Soltesz I (2001) Persistently modified h-channels after complex febrile seizures convert the seizure-induced enhancement of inhibition to hyperexcitability. Nat Med 7:331–337

Chen Y, Yu FH, Surmeier J, Scheuer T, Catterall WA (2006) Neuromodulation of Na^+ channel slow inactivation via cAMP-dependent protein kinase and protein kinase C. Neuron 49:409–420

Colquhoun D, Sigworth FJ (1983) Fitting and statistical analysis of single-channel records. In: Sackmann B, Neher E (eds), Single-Channel Recording. New York: Plenum Press, pp 191–264

Cox DR, Lewis PAW (1966) The Statistical Analysis of Series of Events. Methuen, London

English BP, Min W, Oijen AM, Lee KT, Luo G, Sun H, Cherayil BJ, Kou SC, Xie S (2005) Ever-fluctuating single enzyme molecules: Michaelis-Menten equation revisited. Nat Chem Biol 2:87–94

Goldin A (2003) Mechanisms of sodium channel inactivation. Curr Opin Neurobiol 13:284–290

Grant AO, Starmer CF, Strauss HC (1983) Unitary sodium currents in cardiac myocytes in rabbit. Circ Res 53:823–829

Hamill OP, Neher E, Sackman B, Sigworth FJ (1981) Improved patch-clamp techniques for high-resolution current recording from cells and cell-free membrane patches. Pfluegers Arch 391:85–100

Hille B (2001) Ionic Channels in Excitable Membranes, 3rd ed. Sunderland, MA: Sinauer Associates

Katsumata T, Muramatsu H, Nakamura H, Nishiyama Y, Aloki Y, Katayama Y (2003) Neuro-protective effect of NS 7, a novel Na and Ca channel blocker, in a focal ischemic model in the rat. Brain Res 969:168–174

Kirsch GE, Skattebol A, Possani LD, Brown AM (1989) Modification of Na channel gating by a scorpion toxin from *Tityus serrulatus*. J Gen Physiol 93:67–83

Kohling R (2002) Voltage-gated sodium channels in epilepsy. Epilepsia 43:1278–1295

Kunze DL, Lacarda AE, Wilson DL, Brown AM (1985) Cardiac sodium currents and the inactivating, reopening, and waiting properties of single cardiac Na channel. J Gen Physiol 86:691–719

Labarca P, Rice JA, Fredkin DA, Montal M (1985) Kinetic analysis of channel gating: application to the cholinergic receptor channel and the chloride channel from *Torpedo californica*. Biophys J 47:469–478

Lerch HP, Rigler R, Mikhailov AS (2005) Functional conformational motions in the turnover cycles of cholesterol oxidase. Proc Natl Acad Sci USA 102:10807–10812

Lian J, Shuai J, Durand DM (2004) Control of phase synchronization of neuronal activity in rat hippocampus. J Neuronal Eng 1:46–54

Ma JY, Li M, Catterall WA, Scheuer T (1994) Modulation of brain Na^+ channels by a G-protein-coupled pathway. Proc Natl Acad Sci USA 91:12351–12355

Majumdar S, Foster G, Sikdar SK (2004) Induction of pseudo-periodic oscillation in voltage-gated sodium channel properties is dependent on the duration of prolonged depolarization. Eur J Neurosci 20:127–143

Majumdar S, Sikdar SK (2005) Fast pseudo-periodic oscillations in the rat brain voltage-gated sodium channel α subunit. J Membr Biol 208:1–14

McCormick DA, Shu Y, Hasenstaub A, Sanchez-Vibes M, Badoual M, Bal T (2003) Persistent cortical activity: mechanisms of generation and effects on neuronal excitability. Cereb Cortex 13:1219–1231

McManus OB, Blatz AL, Magleby KL (1985) Inverse relationship of the durations of adjacent open and shut intervals for Cl and K channels. Nature 317:625–627

Mickus T, Jung H-Y, Spruston N (1999) Properties of slow, cumulative sodium channel inactivation in rat hippocampal CA1 pyramidal neurons. Biophys J 76:846–860

Miyamato K, Kanaori K, Nakagawa T, Kuroda Y (2001) Solution structures of the inactivation gate particle peptides of rat brain type IIA and human heart sodium channels in SDS micelles. J Peptide Res 57:193–203

Nuss HB, Balser JR, Orias DW, Lawrence JH, Tomaselli GF, Marban E (1996) Coupling between fast and slow inactivation revealed by analysis of a point mutation (F1304Q) in μ1 rat skeletal muscle sodium channels. J Physiol 494:411–429

O'Reilly JP, Wang SY, Wang GK (2001) Residue-specific effects on slow inactivation at V787 in D2-S6 of Nav1.4 sodium channels. Biophys J 81:2100–2111

Ong BH, Tomaselli GF, Balser JR (2000) A structural rearrangement in the sodium channel pore linked to slow inactivation and use dependence. J Gen Physiol 116:653–661

Patlak J, Horn R (1982) Effect of *N*-bromoacetamide on single sodium channel currents in excised membrane patches. J Gen Physiol 79:333–351

Rahamimoff R, Edry-Schiller J, Fraenkel MR, Butkevich A, Ginsburg S (1995) Oscillation in the activity of a potassium channel at the pre-synaptic nerve terminal. J Neurophysiol 73:2448–2458

Reyes A (2001) Influence of dendritic conductances on the input output properties of neurons. Annu Rev Neurosci 24:653–675

Rohl CA, Boeckman FA, Baker C, Scheuer T, Catterall WA, Klevit RE (1999) Solution structure of the sodium channel inactivation gate. Biochemistry 38:855–861

Rutecki PA, Yang Y (1998) Ictal epileptiform activity in the CA3 region of hippocampal slices produced by pilocarpine. J Neurophysiol 79:3019–3029

Sachs F, Neil J, Barkakati N (1982) Instruments and techniques: the automated analysis of data from single ionic channels. Pfluegers Arch Eur J Physiol 395:331–340

Sanhueza M, Bacigalupo J (2005) Intrinsic sub-threshold oscillations of the membrane potential in pyramidal neurons of the olfactory amygdala. Eur J Neurosci 22:1618–1626

Sarkar SN, Adhikari A, Sikdar SK (1995) Kinetic characterization of rat brain type IIA sodium channel alpha-subunit stably expressed in a somatic cell line. J Physiol 488:633–645

Segal MM (1994) Endogenous burst underlie seizure-like activity in solitary excitatory hippocampal neurons in micro cultures. J Neurophysiol 72:1874–1884

Sigworth FJ, Neher E (1980) Single Na^+ channel currents observed in cultured rat muscle cells. Nature 287:447–449

Su H, Sochivko D, Becker A, Chen J, Jiang Y, Yaari Y, Beck H (2002) Up regulation of a T-type Ca^{2+} channel causes a long-lasting modification of neuronal firing mode after status epilepticus. J Neurosci 22:3645–3655

Sunderman ER, Zagotta WN (1999) Mechanism of allosteric modulation of rod cyclic nucleotide-gated channels. J Gen Physiol 113:602–620

Toib A, Lyakhov V, Marom S (1998) Interaction between duration of activity and time course of recovery from slow inactivation in mammalian brain Na^+ channels. J Neurosci 18:1893–1903

Tsubokawa H, Offermanns S, Simon M, Kano M (2000) Calcium-dependent persistent facilitation of spike back-propagation in the CA1 area of pyramidal neurons. J Neurosci 20:4878–4884

Venkataramanan L, Kuk R, Sigworth FJ (1998) Identification of hidden Markov models for ion channel currents-part II: state dependent excess noise. IEEE Trans Signal Proc 46:1916–1929

Venkataramanan L, Kuk R, Sigworth FJ (2000) Identification of hidden Markov models for ion channel currents-part III: band limited, sampled data. IEEE Trans Signal Proc 48:376–385

Venkataramanan L, Sigworth FJ (2002) Applying hidden Markov models to the analysis of single ion channel activity. Biophys J 82:1930–1942

Vilin YY, Fujimoto E, Ruben PC (2001) A single residue differentiates between human cardiac and skeletal muscle Na^+ channels. Biophys J 80:2221–2230

Vlad MO, Moran F, Schneider FW, Ross J (2002) Memory effects and oscillations in single-molecule kinetics. Proc Natl Acad Sci USA 99:12548–12555

Wang G, Covarrubias M (2006) Voltage-gated gating rearrangements in the intracellular T1-T1 interface of a K^+ channel. J Gen Physiol 127:391–400

Waxman SG, Dib-Hajj S, Cummins TR, Black JA (1999) Sodium channels and pain. Proc Natl Acad Sci USA 96:7635–7639

Wu MF, Pang ZP, Zhuo M, Xu ZC (2005) Prolonged membrane potential depolarization in cingulated pyramidal cells after digit amputation in adult rats. Mol Pain 1:1–23

Xu ZC (1995) Neurophysiological changes of spiny neurons in rat neostriatum after transient forebrain ischemia: an in vivo intracellular recording and staining study. Neuroscience 67:823–836

Zheng J, Venkataramanan L, Sigworth FJ (2001) Hidden Markov model analysis of intermediate gating steps associated with the pore gate of Shaker potassium channels. J Gen Physiol 118:547–562